



DOI: <https://doi.org/10.26628/simp.wtr.v96.1176.4-15>

Original Article

# Selected properties of single-sided resistance spot welded joints on 18650 battery tab

Krzysztof Bieliszczuk  \* and Magdalena Zyskowska 

Department of Joining Engineering, Faculty of Mechanical and Industrial Engineering, Warsaw University of Technology, Narbutta 85, 02-524 Warsaw, Poland  
magdalena.zyskowska.stud@pw.edu.pl (M.Z.)

\* Correspondence: krzysztof.bieliszczuk@pw.edu.pl

Received: 11.11.2023; Accepted: 28.12.2023; Published: 03.01.2024

**Abstract:** The aim of this study was to characterize selected properties of joints made by single-sided serial resistance spot welding of 0.15 mm thickness Hilumin connectors to the negative terminal of LGDBHG21865 lithium-ion cylindrical battery cell. Welding process was performed using production parameters to properly represent actual manufacturing conditions. Mechanical properties of the joints were examined by means of tensile stress test and microhardness measurements while additional studies include metallographic analysis of the joint cross sections by means of optical and scanning microscopy. Energy dispersive spectroscopy was performed in order to determine surface distribution of elements within the weld nugget. Studies confirmed suitable microstructure of welded joints, repeatability of the welding process and proper selection of the welding parameters.

**Keywords:** electric batteries joints; spot welding; lithium ion; resistance welding; series welding

## Introduction

Recent changes in environmental laws are rising awareness of climatic changes puts pressure on manufacturing industry to constantly develop new ways to electrify their product and production facilities. Currently the only feasible way to achieve this is using battery powered devices. To achieve this goal cost-effective methods of battery pack manufacturing need to be constantly developed. Most common type of battery cells used for battery packs manufacturing are 18650 lithium-ion cylindrical cells. However, to meet the requirements for larger nominal voltage, capacity and rated current cells of this type need to be interconnected into larger battery packs with the use of joining processes such as laser welding, ultrasonic welding, wire bonding and resistance spot welding[1]. Laser welding requires high initial investment and extensive process development [2-4]. Ultrasonic welding requires high core pack rigidity due to forces involved and generates large amount of heat [5-7] that can lead to cell damage. Wire bonding is very susceptible to changes in battery pack geometry and state of the battery case surface [8,9]. Resistance welding does not require relatively high initial investment [10,11] and allows for use of manual labor or high level of automation depending on production needs. It requires no extensive process development, surface preparation and in situ monitoring of the process does not require complicated measuring equipment [12], [13]. Due to this it is the method most used for interconnecting of battery cells in small to medium battery pack manufacturing.

Resistance spot welding is a thermoelectrical fusion welding process [14] which can be characterized by three steps. At first joint materials are pushed together by the electrodes. Next the current flow is introduced between two electrodes through the joined materials. This is associated with generation of Joule-Lenz heat at the materials interface area, which is characterized by increased resistance. Generated heat leads to melting and then blending of both materials. As the last step current flow is stopped and the joint is allowed to recrystallize under pressure. This results in formation of a permanent connection between the joined materials.

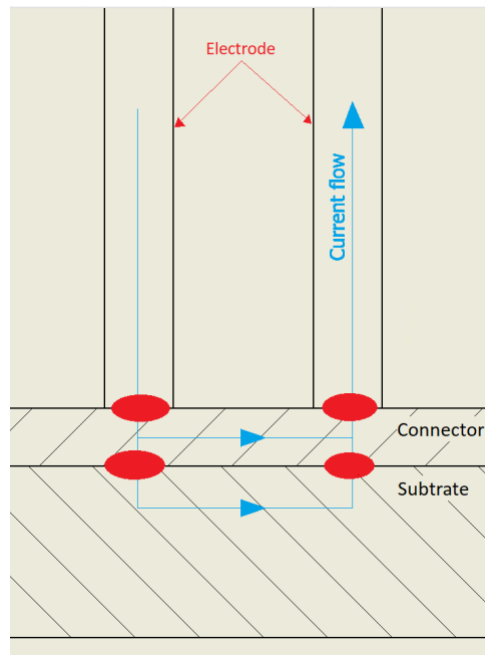


**Fig. 1.** Current flow in process of one side series spot welding

One of resistance welding methods used in battery pack manufacturing is series spot welding. This process occurs through passing of welding current between two parallel electrodes contacting one of the welded materials. Current passes through the connector material to the substrate material resulting in generation of heat on the electrode-connector interface and connector-substrate interface as shown on Figure 1. This method is limited to thin connectors, but its main advantages are the ability to make a connection with access to just one side of the joined materials and the fact that the weld is formed mainly in the material on the electrodes side. This is crucial since battery shell melt through leads to its damage and can result in cell thermal runaway and consequently a fire [15-16].

## Materials and Methods

This study is focused on characterization of selected properties of one side series spot welded joints between 0.15 mm Hilumin, which is a kind of nickel-plated DC04 steel, connector, and 0.3 mm thick negative terminal of LG DB HG2 18650 battery cells. Materials and welding parameters have been taken from production to properly illustrate a real manufacturing process. DC04 steel chemical composition can be seen in Table 1. Battery shell material has not been specified by the manufacturer. The material most used in battery shell production is also Hilumin or other brands of nickel-plated low carbon deep draw steel.

**Table 1.** Chemical composition of Hilumin [17]

	C	Mn	P	S	Al	Si	B
<b>Content [wt. %]</b>	<b>0.047</b>	<b>0.235</b>	<b>0.011</b>	<b>0.010</b>	<b>0.059</b>	<b>0.002</b>	<b>0.002</b>

**Table 2.** Welding parameters and measured welding current

Parameter	Squeeze [ms]	Voltage [V]	Welding time [ms]	Squeeze force [N]	Current RMS [A]	Current peak [A]
<b>Value</b>	<b>30</b>	<b>140</b>	<b>2.1</b>	<b>28</b>	<b>1850</b>	<b>2250</b>

Welding parameters have been presented in Table 2. Squeeze is a time that the materials are pressed together before the welding current is activated. Process on the machine used in this study is regulated to keep the set, constant value of welding voltage for the set amount of welding time. Squeeze force is set manually by spring tensioner and was verified using AXIS FB1k tensimeter. Peak and RMS current are

correlated with set voltage by Ohm's law and were measured during the welding process with Miyachi M-122A weld checker.

Machine used for welding was Poron FC-1200-5 as seen on Figure 1 (a) equipped with copper electrodes Figure 1 (b). Welds were made on battery negative terminal in 2 lines as seen on Figure 1 (c).

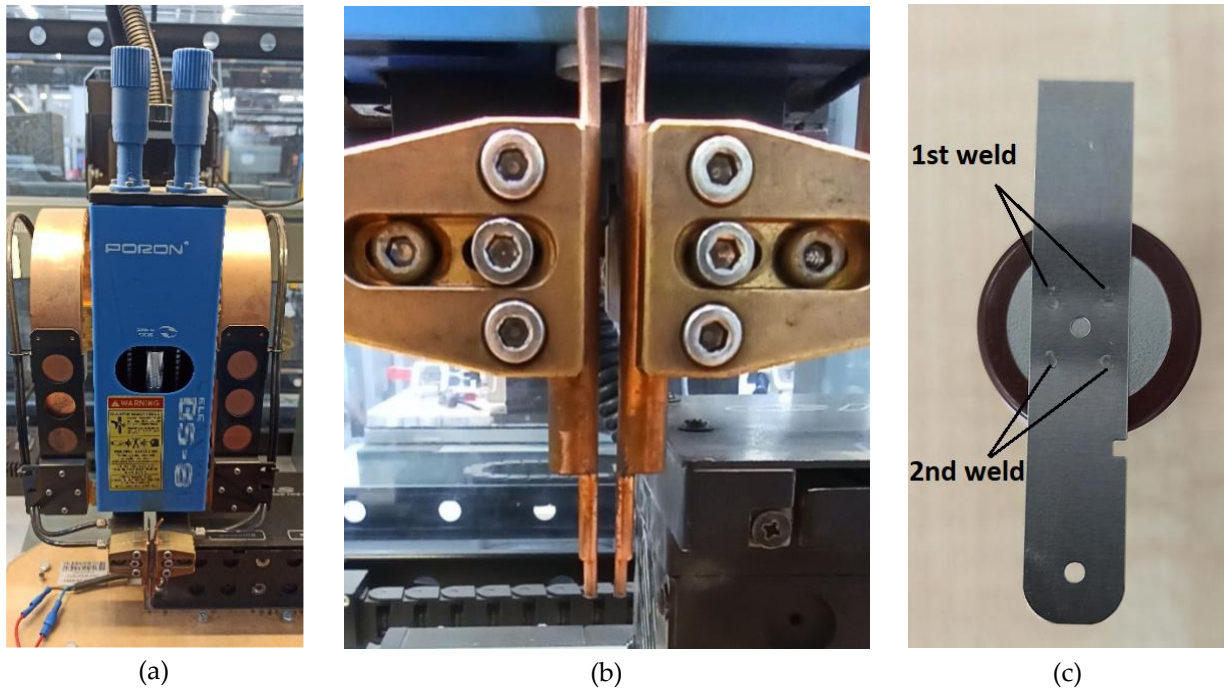


**Fig. 2.** (a) Welding head – general view (b) Electrodes, (c) Weld sequence on negative battery terminal

Electrodes were made of Wirbalit HF which is a CuCr1Zr alloy. Electrode material has been presented in Table 3. Diameter of the electrodes tips was 1.2 mm and the distance between electrodes was 3.65 mm center to center as seen on Figure 3.

**Table 3.** Wirbalit HF composition as per manufacturer specification [18]

	Cu	Cr	Zr
<b>Content [wt. %]</b>	99.27	0.65	0.08

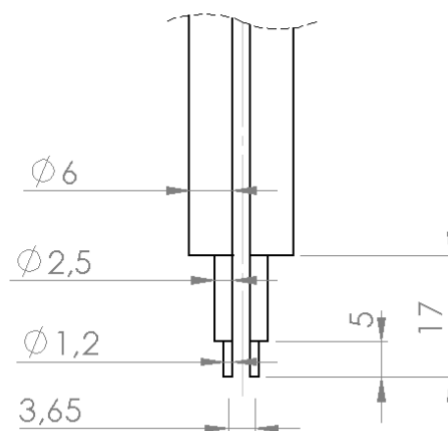


**Fig. 3.** Welding electrodes geometry and dimensions.

Metallographic observations and microhardness measurements were carried out on samples taken perpendicularly to the cell height in such a way, to include both welds made during single weld cycle as in Figure 4 (a).

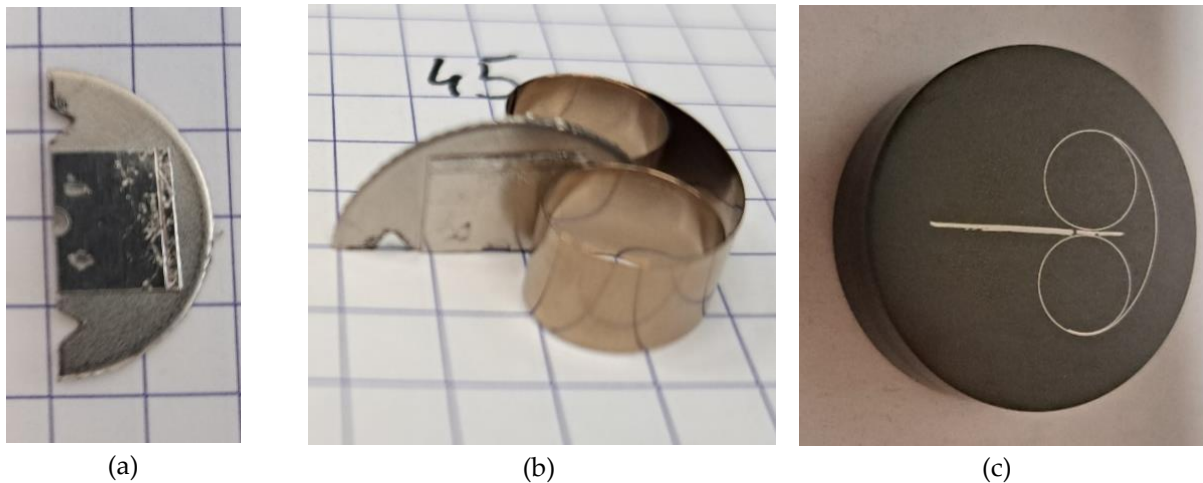


**Fig. 4.** (a) Sample cutout for mounting, (b) Sample orientation during mounting, (c) Mounted and polished sample

Samples for SEM were mounted in QATM Duroplast electroconductive hot mounting powder and grinded using #80, 200, 400, 800, 1200, 2500 silicon carbide papers. Polishing was conducted using Struers AP-A 1  $\mu\text{m}$  agglomerated alpha alumina powder on MD-Chem grinding disc. Sample prepared for SEM can be seen on Figure 4 (c). Samples used for optical microscopy were cold mounted in Epidian 5 transparent resin and prepared in the same way. Additionally, to ensure proper plane of cross section triangular marks were cut in the samples at the depth of analyzed joints. The final step in the preparation of the spot-welded samples was etching with 5% Nital.

To analyze the chemical composition of materials ThermoFisher Scientific Axia ChemiSEM Scanning Electron Microscope was used. Optical microscopy was carried out on Olympus BX51M microscope using Olympus Stream Essential software. Vickers microhardness was measured using Leitz microhardness tester with 10p (0.01 kgf, 0.098 N) test weight.

Tensile strength was tested on 5000 N measuring sensor set to 500 N measurement range with speed set to 2 mm/min. Cell was clamped in 3 jaw chuck while the connector was clamped using a spacer the width of 6 mm as seen on Figure 5.



**Fig. 5.** Sample clamping on tensile strength measuring machine

## Results and Discussion

### Tensile stress test results

In order to confirm repeatability of the welding process tensile strength tests were performed on a group of 10 battery cells.

**Table 4.** Results of breaking load measurement for spot welded joints on battery cells

Sample no.	1	10	11	12	15	16	17	21	22	23
Fmax [N]	145.3	197.2	190.5	155.5	168.5	190.3	185.7	173.0	200.8	184.7
Median [N]	185.2									
Mean [N]	179.2									
Std dev [N]	17.3									
St dev [%] med	9.3									

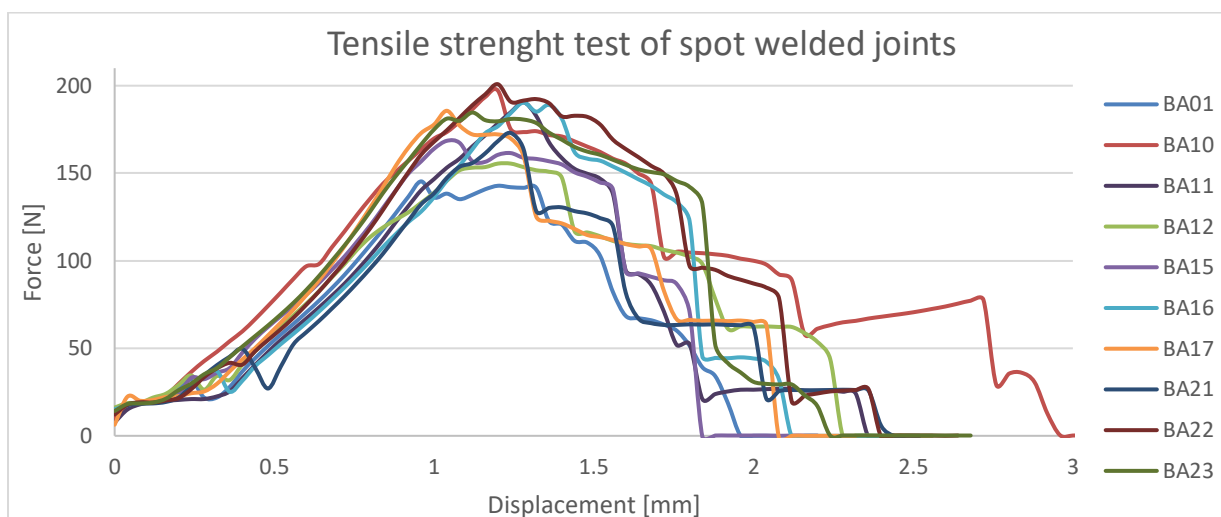


**Fig. 6.** Tensile stress curves for spot welded joints on battery cells

Breaking load has been presented in table 4 while stress-strain curves have been presented in Figure 6. Standard deviation of 9.3% in the force value indicates the repeatability of the welding process while breaking load of 185.2 N (median) is on a satisfactory level. Force curves indicate highly ductile fracture with multiple peaks representing failures of separate welds.

Pre fracture macro images seen on Figure 7 (a) have been compared with their corresponding post fracture images on Figure 7 (b). This revealed that the fracture occurred in the connector, on the weld outside boundary. This is a desired failure mode indicating a proper nugget formation.



**Fig. 7.** Macro images of welds before (a) and after (b) tensile strength tests

Remnants of the welds have been ground flat to properly measure the surface area of the connection as seen on Figure 8.

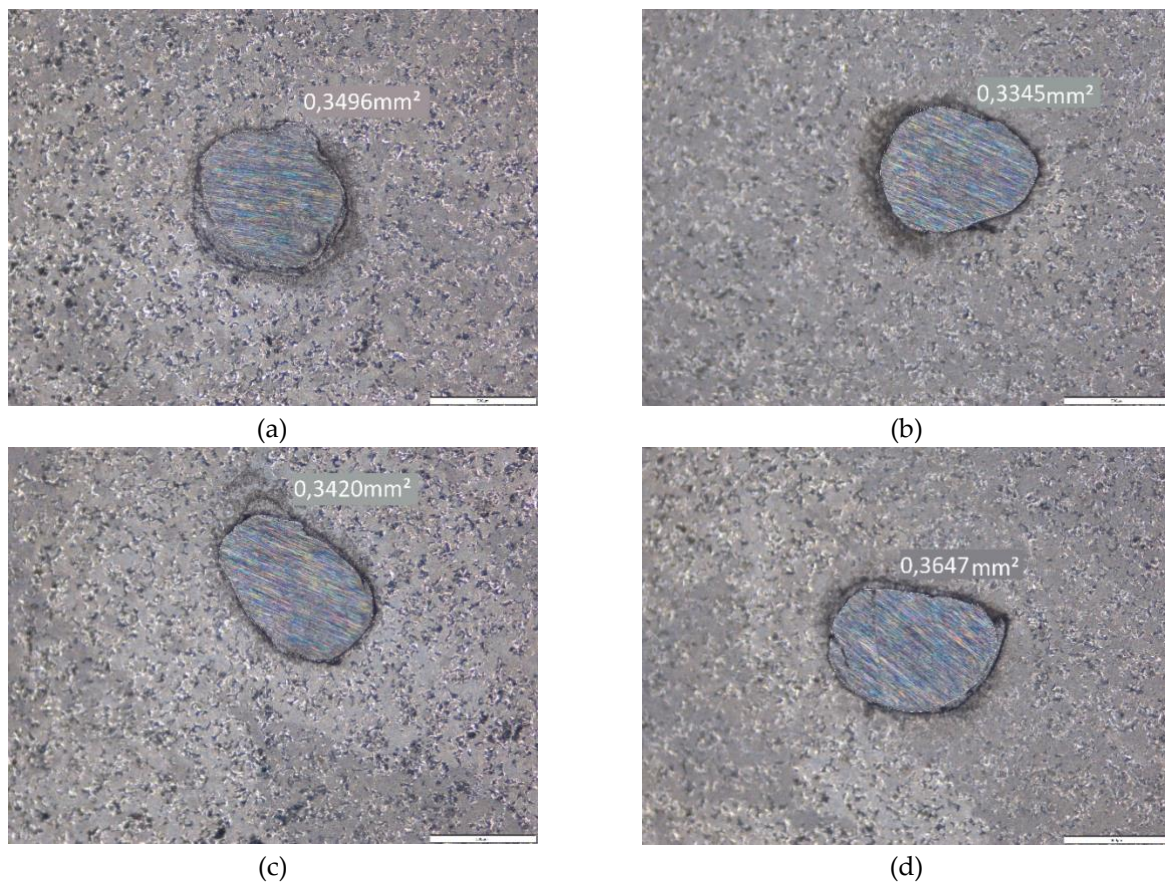


**Fig. 8.** Weld cross sections measured on sample number 17

Results of weld surface area have been presented in Table 4. Records that are marked as N/A have been ground too deep to properly measure the surface area and since have been excluded from the table.

**Table 4.** Results of post fracture weld surface area measurements

Sample no.	1	10	11	12	15	16	17	21	22	23	
Weld 1 area [mm <sup>2</sup> ]	0.1010	0.3541	0.2748	0.3546	0.4048	0.4208	0.3496	0.2236	0.3592	0.1010	
Weld 2 area [mm <sup>2</sup> ]	0.2257	0.3981	0.1985	0.3772	0.3141	0.4252	0.3420	0.3133	0.3665	0.2257	
Weld 3 area [mm <sup>2</sup> ]	0.2333	N/A	0.3700	0.3713	0.3963	0.4548	0.3647	0.2224	N/A	0.2333	
Weld 4 area [mm <sup>2</sup> ]	0.3528	N/A	0.3978	0.3566	0.3804	0.3273	0.3345	0.2809	N/A	0.3528	
Median [mm <sup>2</sup> ]						0.3543					
Mean [mm <sup>2</sup> ]						0.3328					
Std. Dev. [mm <sup>2</sup> ]						0.0745					
Std. Dev. [%]						21.0					

Comparison of breaking load values and weld area cross sections revealed that sample number 1 deviates from the rest of the samples, but otherwise remaining samples are consistent. Median surface area measured was 0.3543 mm<sup>2</sup> which indicates that the weld pool diameter was about half the value of the electrode diameter. This positively evaluates the welding parameters and meets the desired specification.

### *Metallographic Investigation*

In order to properly examine the joint area metallographic cross sections of the selected weld samples were examined under an optical microscope. Observations revealed that the majority of the weld is formed in the connector. Measurements seen on Figure 9 show, that the changes in the cell material structure reaches between 95 and 127  $\mu\text{m}$  deep into the battery cell material from the interface. This ensures, that the welding process does not damage the internal components of the cell.

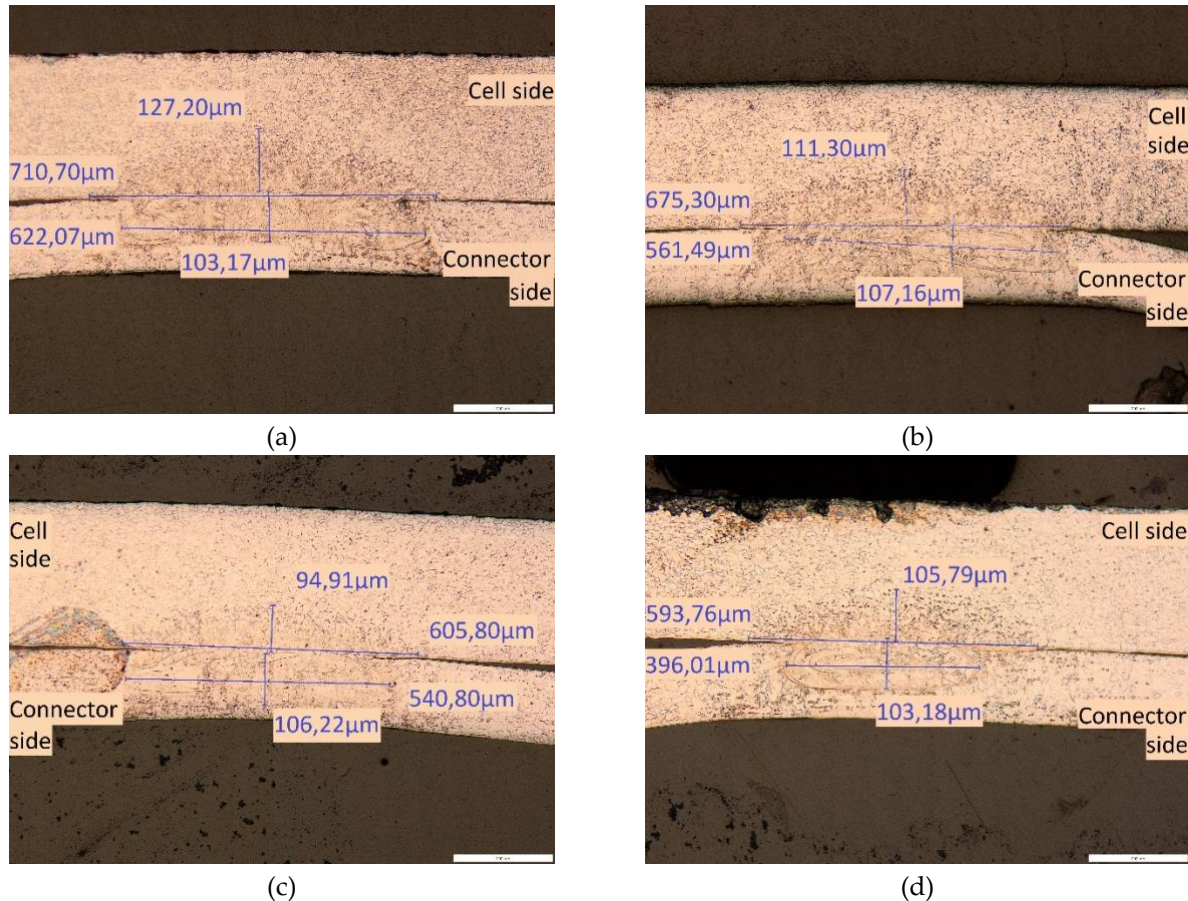


**Fig. 9.** Cross section measurements under optical microscope - x100

Weld pool size varies from 400 to 600  $\mu\text{m}$  in width and has a consistent height of around 105  $\mu\text{m}$ . Heat affected zone (HAZ) is clearly indicated by the structural changes in both the connector and the battery cell material with width varying from 600 to 700  $\mu\text{m}$ . Nickel has been mostly expelled from the interface into the boundaries of the joint. No fractures were observed in the analyzed samples.

### *Scanning Electron Microscopy (SEM) and Energy Dispersive Spectroscopy (EDS)*

SEM imaging revealed changes within the weld area that can be seen on Figure 10 (a).

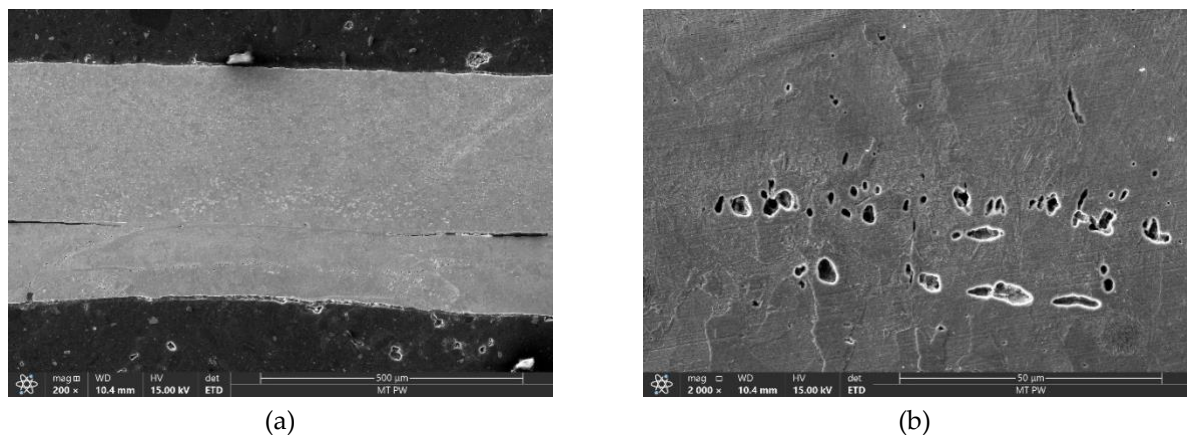


**Fig. 10.** SEM images of one of the samples. (a) pores visible in 200x magnification, (b) pores close up in 2000x magnification

The changes observed within the sample were located on the connector side of the weld in the border of the Heat Affected Zone (HAZ). It can be seen on Figure 10 (b) that the structure of this area did not go through the liquid phase during the weld process. To properly examine those changes area EDS was performed. Results of EDS can be seen on Figure 11 (a) with Iron (b), Carbon (c) and Manganese (d) distribution within the scanned area.

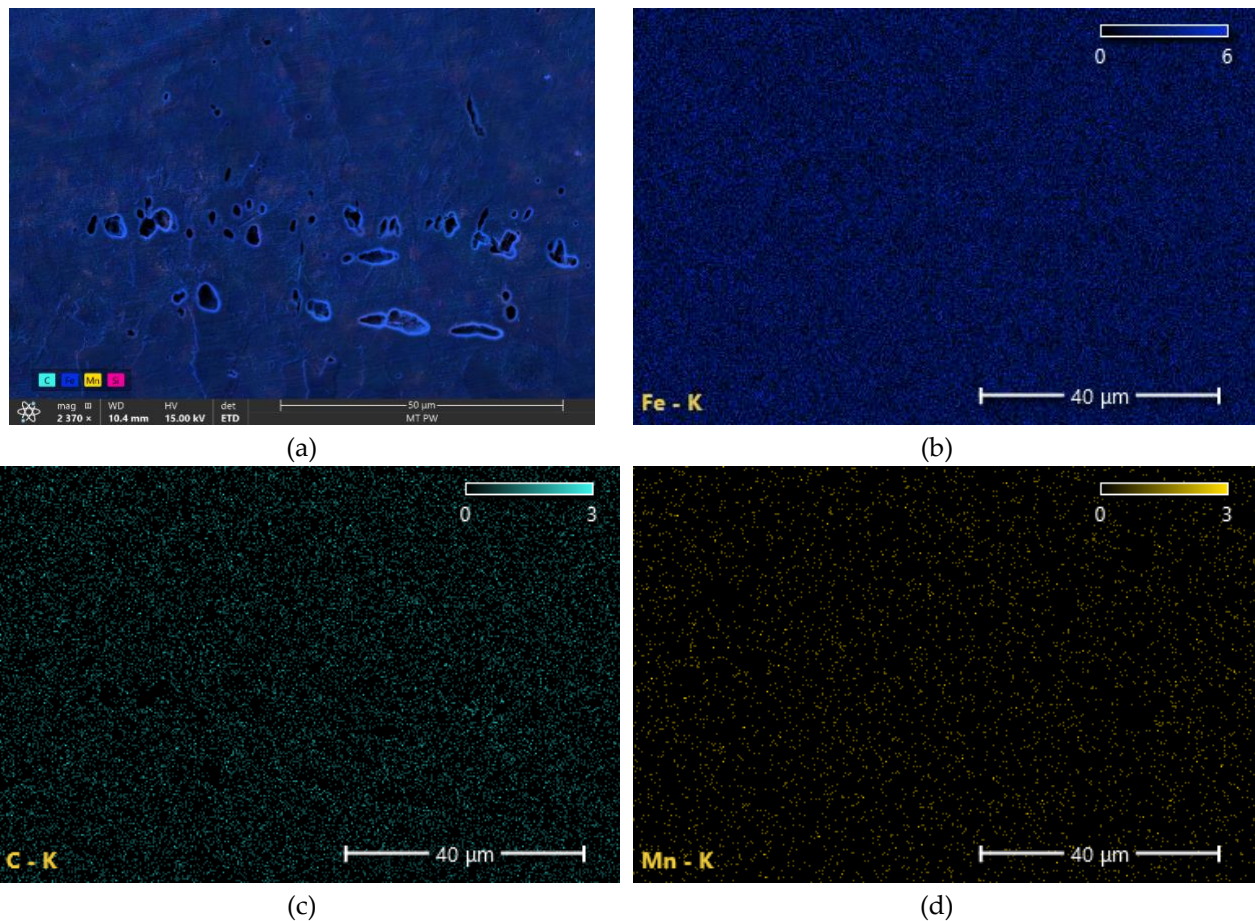


**Fig. 11.** Area EDS results of the changes (a) summary quantity map, (b) Fe count, (c) C count, (d) Mn count

Distribution map revealed that there are no additional elements in comparison with base material. This proves, that the observed changes are porosities. To establish the source of this porosity base material of both the connector and the battery case have been looked at in more detail as seen on Figure 12.

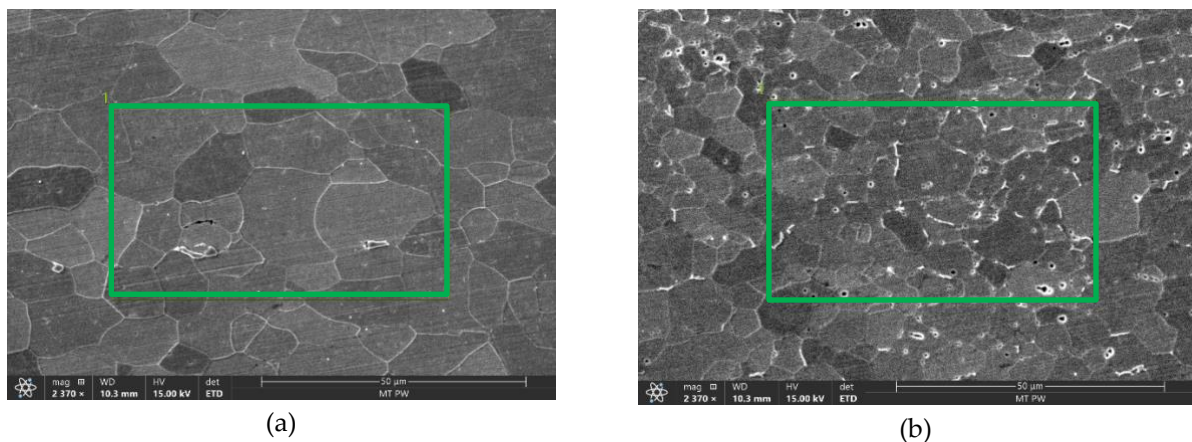


**Fig. 12.** (a) Base material of the Hilumin connector, (b) Base material of the battery cell

Spectrum analysis of elements in the green areas visible on Figure 12 revealed no additional elements beyond iron and carbon. In addition, much more of the porosities were discovered in the battery case material than in the connector material. Those porosities are metallurgical defects of the supplied material that



concentrate on the border of the HAZ and thus should not be considered a welding defect. Spectral analysis plots can be seen on Figure 13.

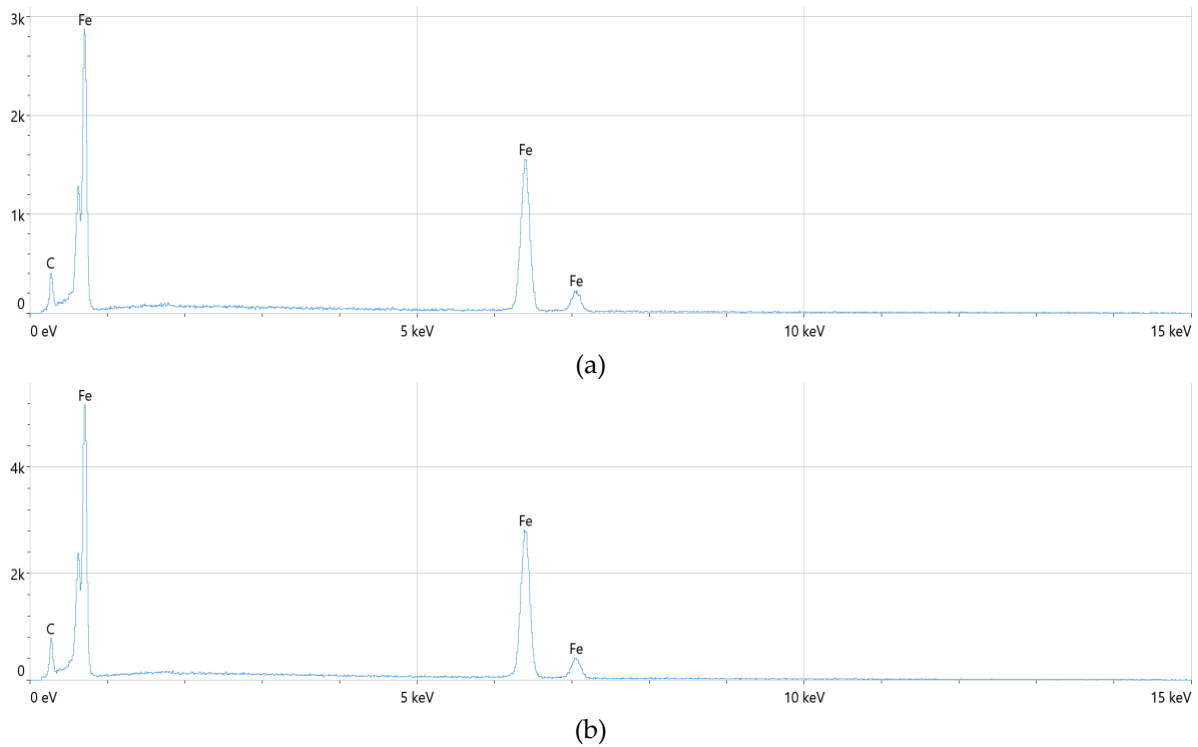


**Fig. 13.** Spectral analysis plots of the base material of the (a) connector and (b) battery case

In order to properly examine the distribution of elements within the weld nugget area and better determine the behavior of nickel during the welding process area EDS was performed as seen on Figure 14.

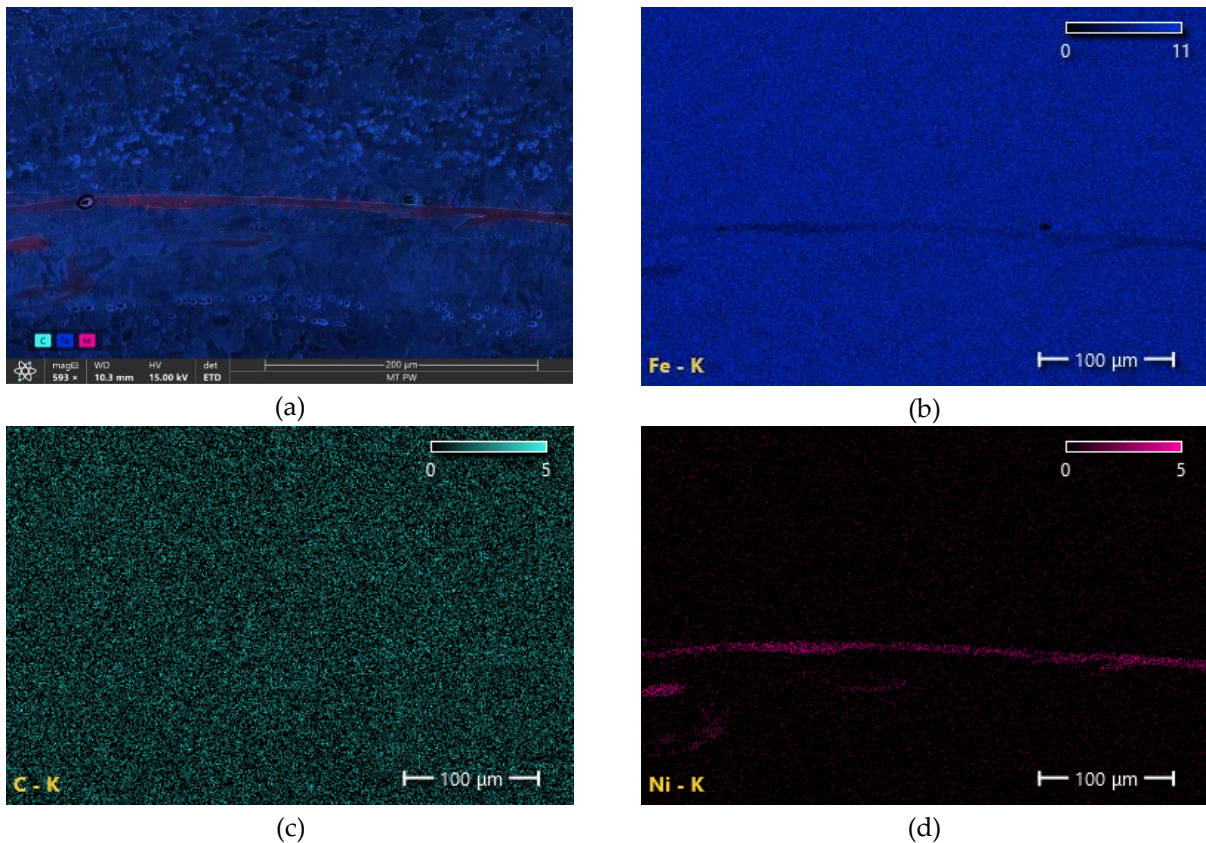


**Fig. 14.** EDS analysis of the weld nugget area (a) summary quantity map, (b) Fe count, (c) C count, (d) Ni count

Results of EDS revealed nickel flow into the pool of molten metal within the weld nugget. Distribution of nickel varies in this area. Areas where nickel diffused into the steel which are characterized by lower nickel

concentration are localized within the weld nugget. Areas where nickel flowed into the base connector material without much diffusion are visible mainly on the edges of the joint.

Line EDS was performed throughout the sample in a line intersecting the middle of the joined materials interface.

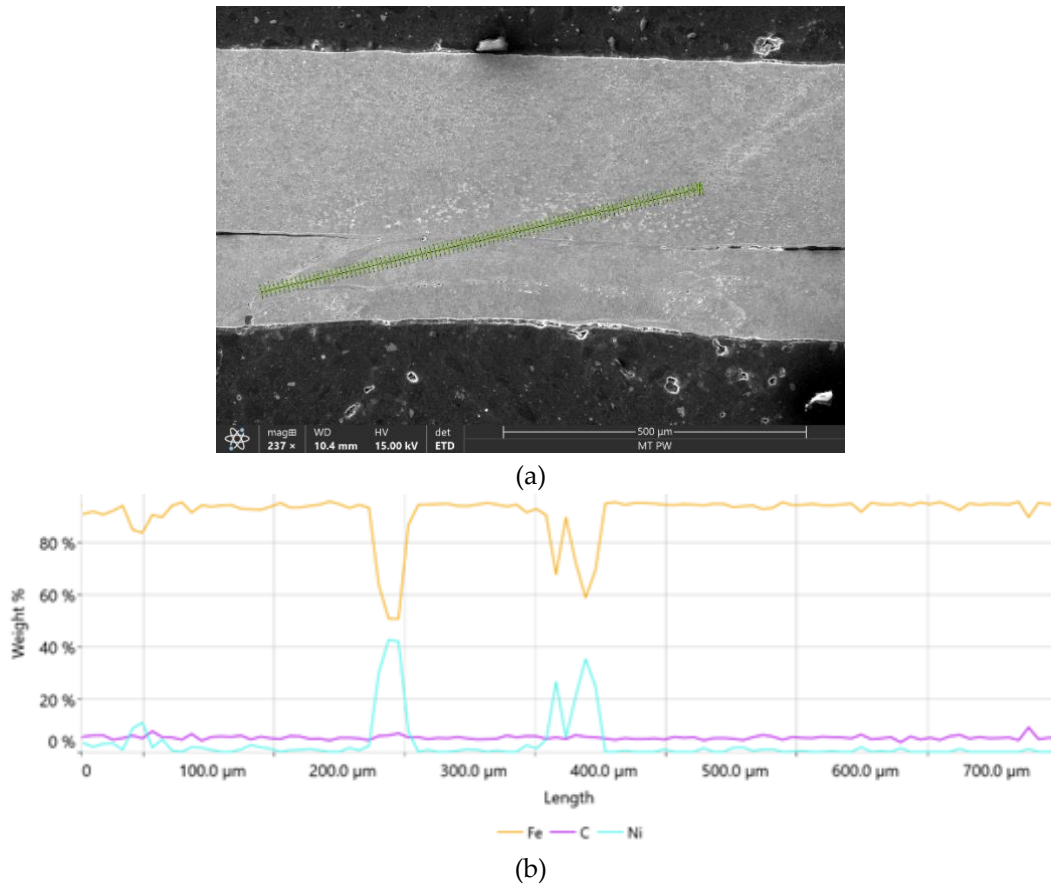


Fig. 15. Line EDS (a) location, (b) linear distribution of elements

Results of line EDS confirmed the results of surface EDS. Elevated nickel content was observed mostly on the material interface area and on the outer edge of the joint on the connector side.

### Microhardness Measurements

Vicker Microhardness (HV0.01) distribution has been measured on one sample due to high repeatability of the welds confirmed by tensile stress test results and metallographic investigations. Microhardness measurements were conducted throughout the sample in one line intersecting the middle point of the material interface as seen on Figure 16. This was consistent with the line spectral analysis seen on Figure 15. Due to small dimensions of analyzed sample and irregular shape of the weld nugget associated with nickel distribution within the sample additional measurement lines had to be abandoned.

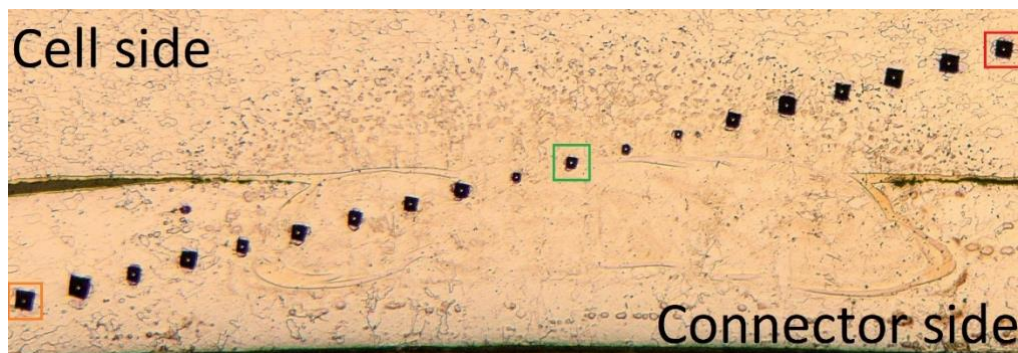


Fig. 16. Microhardness distribution measurement line

Microhardness distribution has been presented in Figure 17. Significant raise in material hardness has been observed in proximity to the material interface. Measurement conducted on the interface (green) indicated lower hardness in this area, which is probably associated with local higher nickel content.

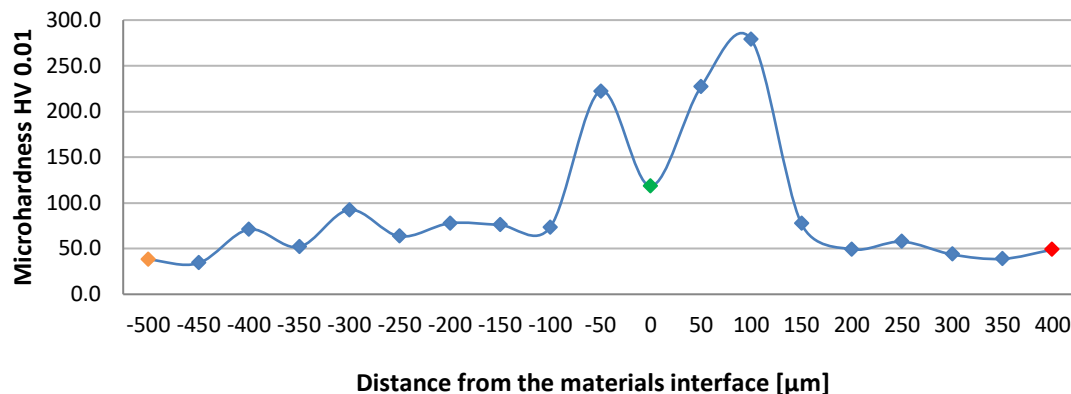


Fig. 17. Microhardness distribution graph

Those result in combination with previous tensile stress tests and metallographic analysis indicate, that despite the grain growth occurring in the area of material interface its hardness did not increase enough to make it prone to cracking. This can be associated with elevated concentration of nickel in this area and overall this connection should be considered a good joint.

## Conclusions

Results of tensile stress test confirmed the repeatability of the welding process. This combined with microstructure analysis and EDS allowed for positive verification of spot-welding parameters selection. Process established in this study can be used as a baseline for further research on the topic of battery cell resistance spot welding. Further research should implement additional numerical simulation of the spot-welding process in order to better understand physical phenomena occurring within the weld area such as process heat distribution and the effect of parameter changes on the welding process. Area of structural changes in the heat affected zone of the battery cell material qualifies this process for studies of battery welding on more complex surface such as the cylindrical battery cell crimp.

**Author Contributions:** conceptualization, K.B. and M.Z.; methodology, K.B.; validation, K.B.; formal analysis, K.B.; investigation, K.B and M.Z.; resources, K.B and M.Z.; data curation, M.Z.; writing—original draft preparation, K.B and M.Z.; writing—review and editing, K.B and M.Z.; visualization, M.Z.; supervision, K.B.; project administration, K.B.

**Funding:** This research received no external funding

**Acknowledgments:** We gratefully acknowledge the support provided by Wamtechnik sp. z o.o., Techniczna 2H Str., 05-500 Piaseczno, Poland, which provided the spot-welding machine and welding supplies used in this study. We would also like to express our gratitude to Warsaw University of Technology, Faculty of Mechanical and Industrial Engineering for providing scientific equipment and facilities needed to complete this study.

**Conflicts of Interest:** The authors declare no conflict of interest.

## References

- [1] Brand M.J.; Schmidt P.A.; Zaeh M.F.; Jossen A. Welding techniques for battery cells and resulting electrical contact resistances, *J Energy Storage*, **2015**, Vol. 1(1), 7–14. <https://doi.org/10.1016/j.est.2015.04.001>
- [2] Alexy A.; Van de Wall D.; Shannon G.; and Boyle M.L. Batteries need strong connections – are resistance, laser and micro TIG welding the best suited joining technologies?, *Biuletyn Instytutu Spawalnictwa*, **2019**, Vol. 2019(1), 53–63. <https://doi.org/10.17729/EBIS.2019.1/6>
- [3] Das A.; Li D.; Williams D., and Greenwood D. Joining Technologies for Automotive Battery Systems Manufacturing, *World Electr. Veh. J.*, **2018**, Vol. 9(2). <https://doi.org/10.3390/wevj9020022>

- [4] Kumar N.; Masters I.; Das A. In-depth evaluation of laser-welded similar and dissimilar material tab-to-busbar electrical interconnects for electric vehicle battery pack, *J Manuf Process*, **2021**, Vol. 70, 78–96. <https://doi.org/10.1016/J.JMAPRO.2021.08.025>
- [5] Li H.; *et al.*, Transient temperature and heat flux measurement in ultrasonic joining of battery tabs using thin-film microsensors, *J Manuf Sci Eng*, **2013**, Vol. 135(5), 78-96. <https://doi.org/10.1115/1.4024816/376585>
- [6] Zhao J.; Li H.; Choi H.; W. Cai, Abell J.A.; and Li X. Insertable thin film thermocouples for in situ transient temperature monitoring in ultrasonic metal welding of battery tabs, *J Manuf Process*, **2013**, Vol. 15(1), 136–140. <https://doi.org/10.1016/J.JMAPRO.2012.10.002>
- [7] Zwicker M.F.R.; Moghadam M.; Zhang W.; and Nielsen C.V. Automotive battery pack manufacturing – a review of battery to tab joining, *Journal of Advanced Joining Processes*, **2020**, Vol. 1, 100017. <https://doi.org/10.1016/J.JAJP.2020.100017>
- [8] Chan Y.H.; Kim J.K.; Liu D.; Liu P.C.K.; Cheung Y.M.; and Ng M.W. Comparative performance of gold wire bonding on rigid and flexible substrates, *Journal of Materials Science: Materials in Electronics*, **2006**, Vol. 17(8), 597–606.
- [9] Sedlmair J.; Mehlmann B.; and Olowinsky A. Laserbonding instead of ultrasonic wire bonding - An alternative joining technology for power applications, **2017 International Conference on Electronics Packaging, ICEP 2017**, pp. 94–96. <https://doi.org/10.23919/ICEP.2017.7939332>
- [10] Masomtob M.; Sukondhasingha R.; Becker J. and Sauer D.U. Parametric Study of Spot Welding between Li-ion Battery Cells and Sheet Metal Connectors, *Engineering Journal*, 2017, Vol. 21(7), 457–473. <https://doi.org/10.4186/ej.2017.21.7.457>
- [11] Kumar N.; *et al.*, In-depth evaluation of micro-resistance spot welding for connecting tab to 18,650 Li-ion cells for electric vehicle battery application, *International Journal of Advanced Manufacturing Technology*, **2022**, Vol. 121(9–10), 6581–6597. <https://doi.org/10.1007/S00170-022-09775-Z/TABLES/10>
- [12] Jou M. Real time monitoring weld quality of resistance spot welding for the fabrication of sheet metal assemblies, *J Mater Process Technol*, **2003**, Vol. 132(1–3), 102–113. [https://doi.org/10.1016/S0924-0136\(02\)00409-0](https://doi.org/10.1016/S0924-0136(02)00409-0)
- [13] Ariyanto A.; *et al.*, Prototype of Resistance Spot Welding Material Preparation to Improve the Quality of Welding Joints, *International Journal of Engineering Business and Social Science*, **2023**, Vol. 1(4), 283–289. <https://doi.org/10.58451/IJEBSS.V1I04.58>
- [14] Angani A.; Hwang H.M.; Cha H.R.; and Kim Y.G. Spot Welding Characteristics on the Manufacturing Method of Li-Ion Battery Packs for Electric Vehicle, *International Conference on Control, Automation and Systems*, **2023**, 878–881. <https://doi.org/10.23919/ICCAS59377.2023.10316836>
- [15] Mallick S.; and Gayen D. Thermal behaviour and thermal runaway propagation in lithium-ion battery systems – A critical review, *J Energy Storage*, **2023**, Vol. 62, 106894. <https://doi.org/10.1016/J.EST.2023.106894>
- [16] Xu B.; Lee J.; Kwon D.; Kong L.; and Pecht M. Mitigation strategies for Li-ion battery thermal runaway: A review, *Renewable and Sustainable Energy Reviews*, **2021**, Vol. 150, 111437. <https://doi.org/10.1016/J.RSER.2021.111437>
- [17] Das A.; Beaumont R.; Masters I.; and Haney P. Macro-Modelling of Laser Micro-Joints for Understanding Joint Strength in Electric Vehicle Battery Interconnects, *Materials*, **2021**, Vol. 14(13), 3552. <https://doi.org/10.3390/MA14133552>
- [18] SVS Schweisstechnik, “Wirbalit HF specification sheet.” Accessed: Dec. 15, 2023. [Online]. Available: [https://www.svs-schweisstechnik.de/files/downloads/wirbalit\\_hf\\_data\\_sheet.pdf](https://www.svs-schweisstechnik.de/files/downloads/wirbalit_hf_data_sheet.pdf)



© 2024 by the authors. Submitted for possible open access publication under the terms and conditions of the Creative Commons Attribution (CC BY) license (<http://creativecommons.org/licenses/by/4.0/>).